Supplement of Hydrol. Earth Syst. Sci., 26, 35–54, 2022
https://doi.org/10.5194/hess-26-35-2022-supplement

Hydrology and Earth System Sciences
Open Access
EGU

Supplement of

How well are we able to close the water budget at the global scale?

Fanny Lehmann et al.

Correspondence to: Fanny Lehmann (fanny.lehmann@bristol.ac.uk)

Supplementary material

Additional figures

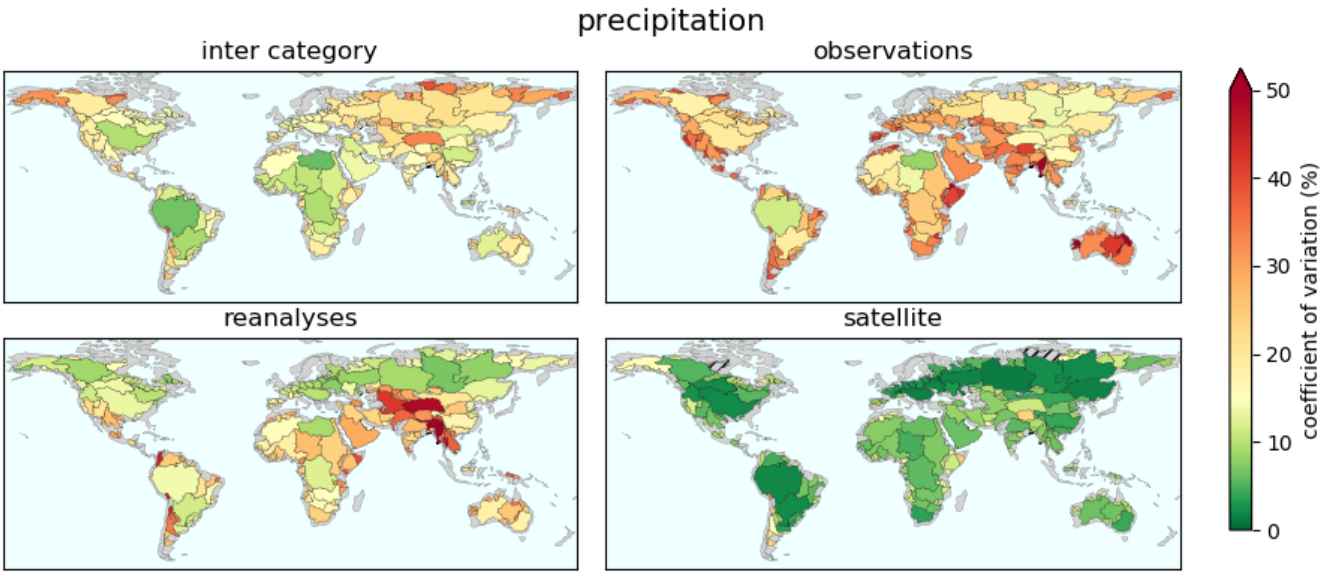

Figure S1. Coefficient of variation between different sets of precipitation datasets. Satellite: TRMM, GPM, and GPCP. Observations: CPC, CRU, and GPCC. Reanalyses: ERA5 Land, JRA55, and MERRA2. Inter-category: mean of satellite, observations, and reanalyses.

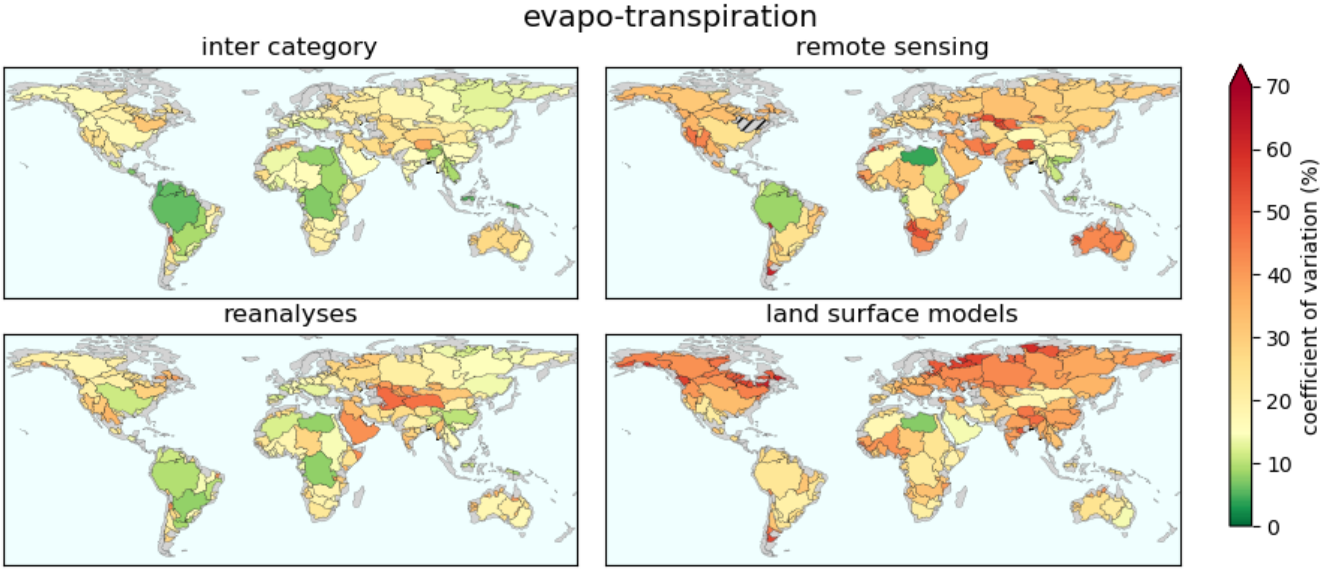

Figure S2. Coefficient of variation between different sets of evapotranspiration datasets. Remote sensing: FLUXCOM, GLEAM, MOD16, and SSEBop. Land surface models: CLSM, Noah, and VIC with versions 2.0 and 2.1. Reanalyses: ERA5 Land, JRA55, and MERRA2. Inter-category: mean of remote sensing, LSMs, and reanalyses.

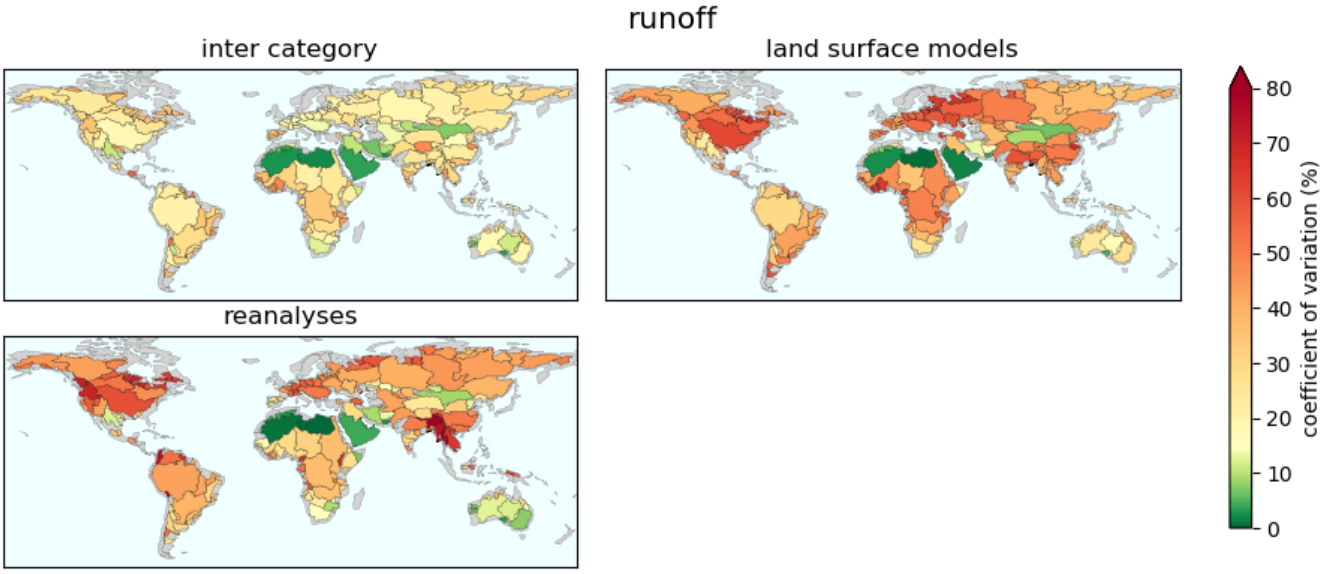

Figure S3. Coefficient of variation between different sets of runoff datasets. Land surface models: CLSM, Noah, and VIC with versions 2.0 and 2.1. Reanalyses: ERA5 Land, JRA55, and MERRA2. Inter-category: GRUN, mean of LSMs, and mean of reanalyses.

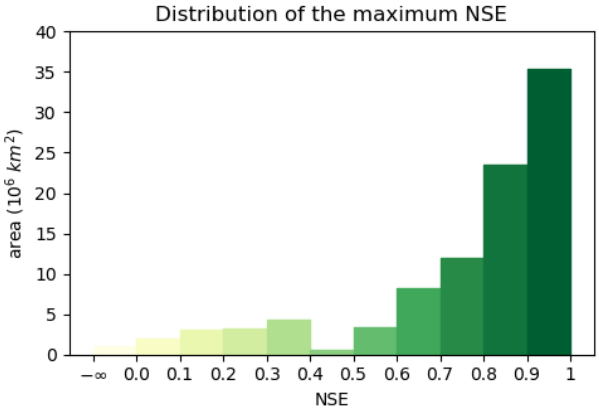

Figure S4. Distribution of the maximum NSE over all combinations in terms of basin area

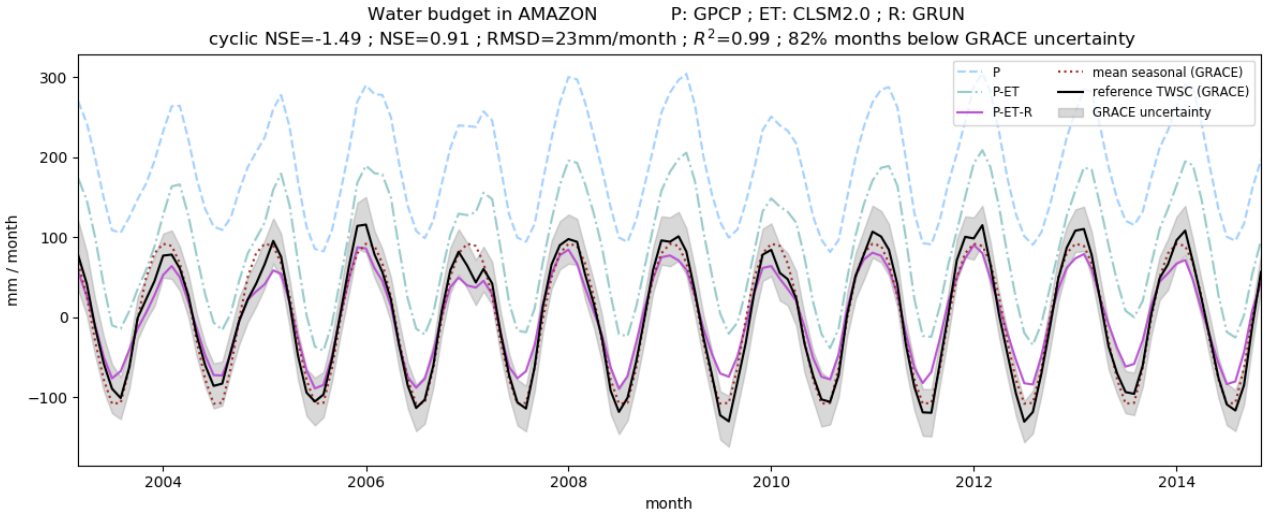

Figure S5. Components of the water budget in the Amazon basin for the combination leading to the highest NSE

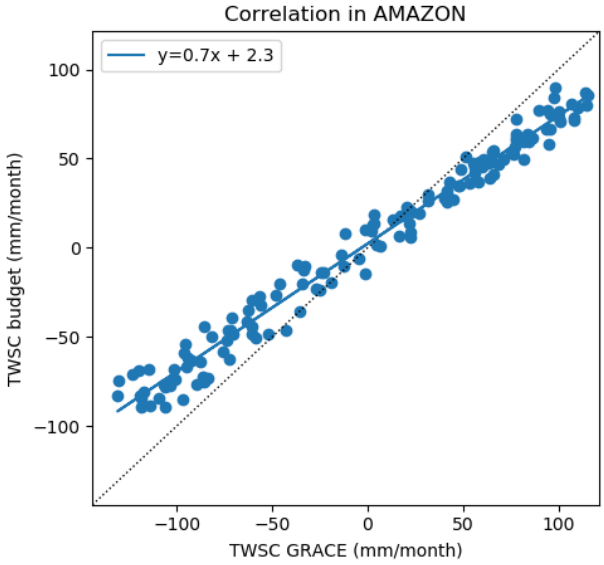

Figure S6. Correlation between monthly values of GRACE TWSC and the budget reconstruction in the Amazon basin, with the combination leading to the highest NSE (NSE=0.92 and cyclostationary NSE=-1.28)

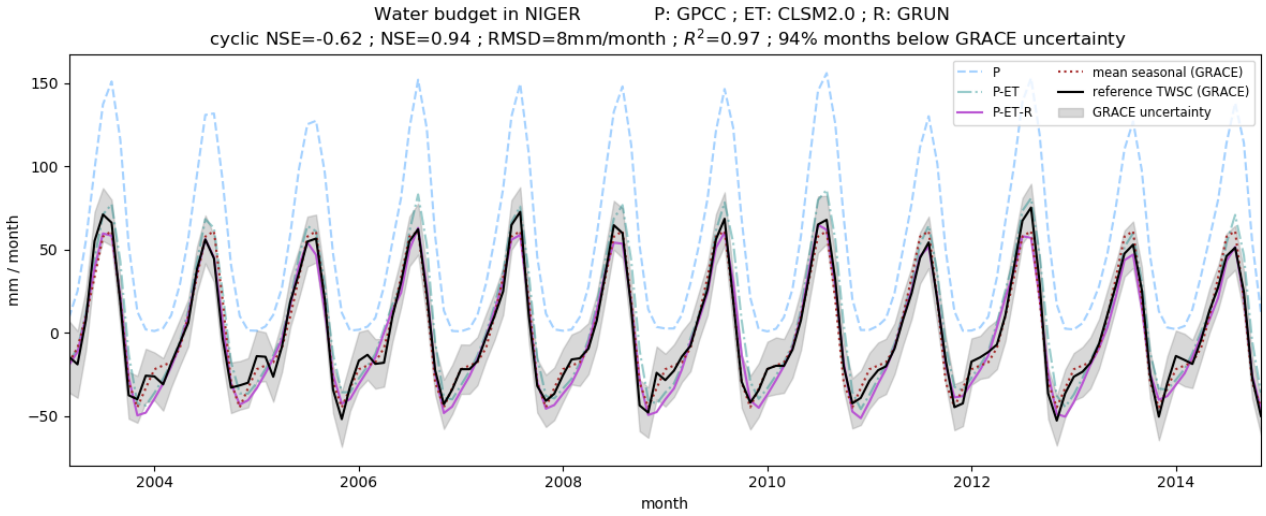

Figure S7. Components of the water budget in the Niger basin for the combination leading to the highest NSE

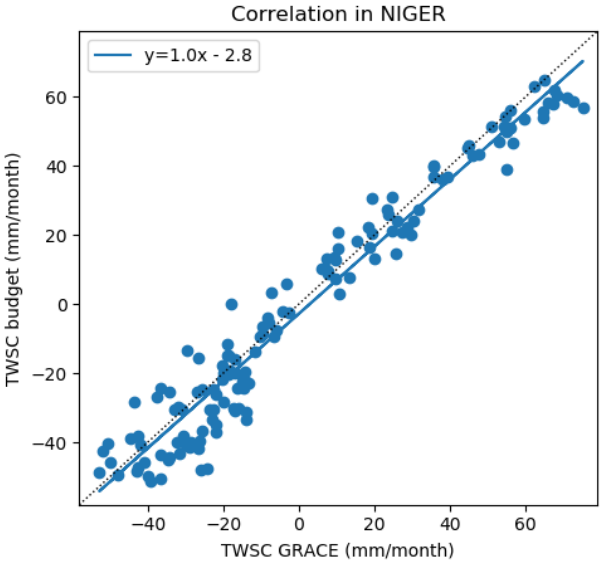

Figure S8. Correlation between monthly values of GRACE TWSC and the budget reconstruction in the Niger basin, with the combination leading to the highest NSE (NSE=0.94 and cyclostationary NSE=-0.62)

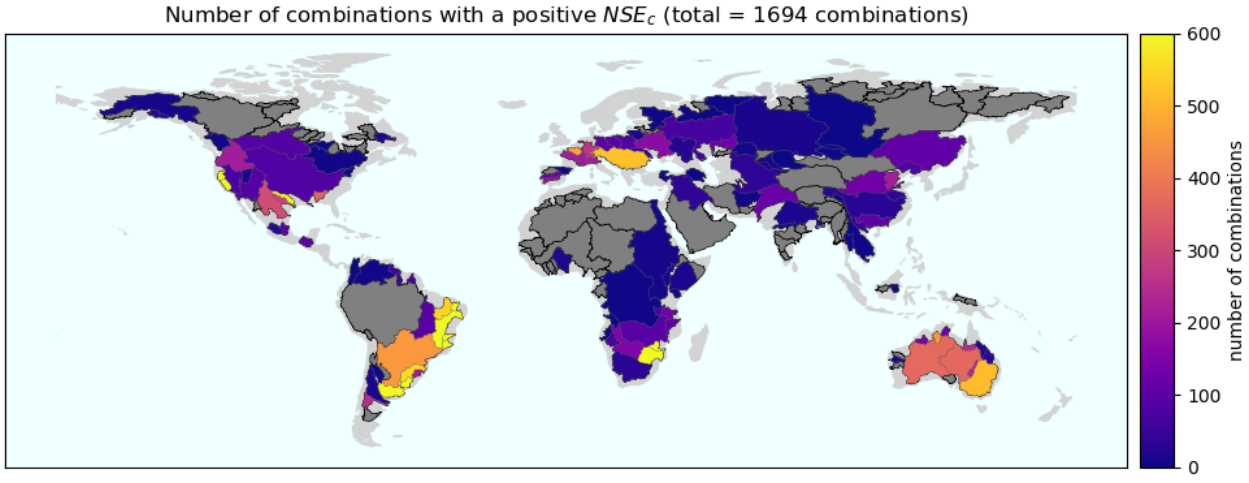

Figure S9. Number of combinations yielding a positive cyclostationary NSE in each basin. Grey means that no combination achieved a positive value.

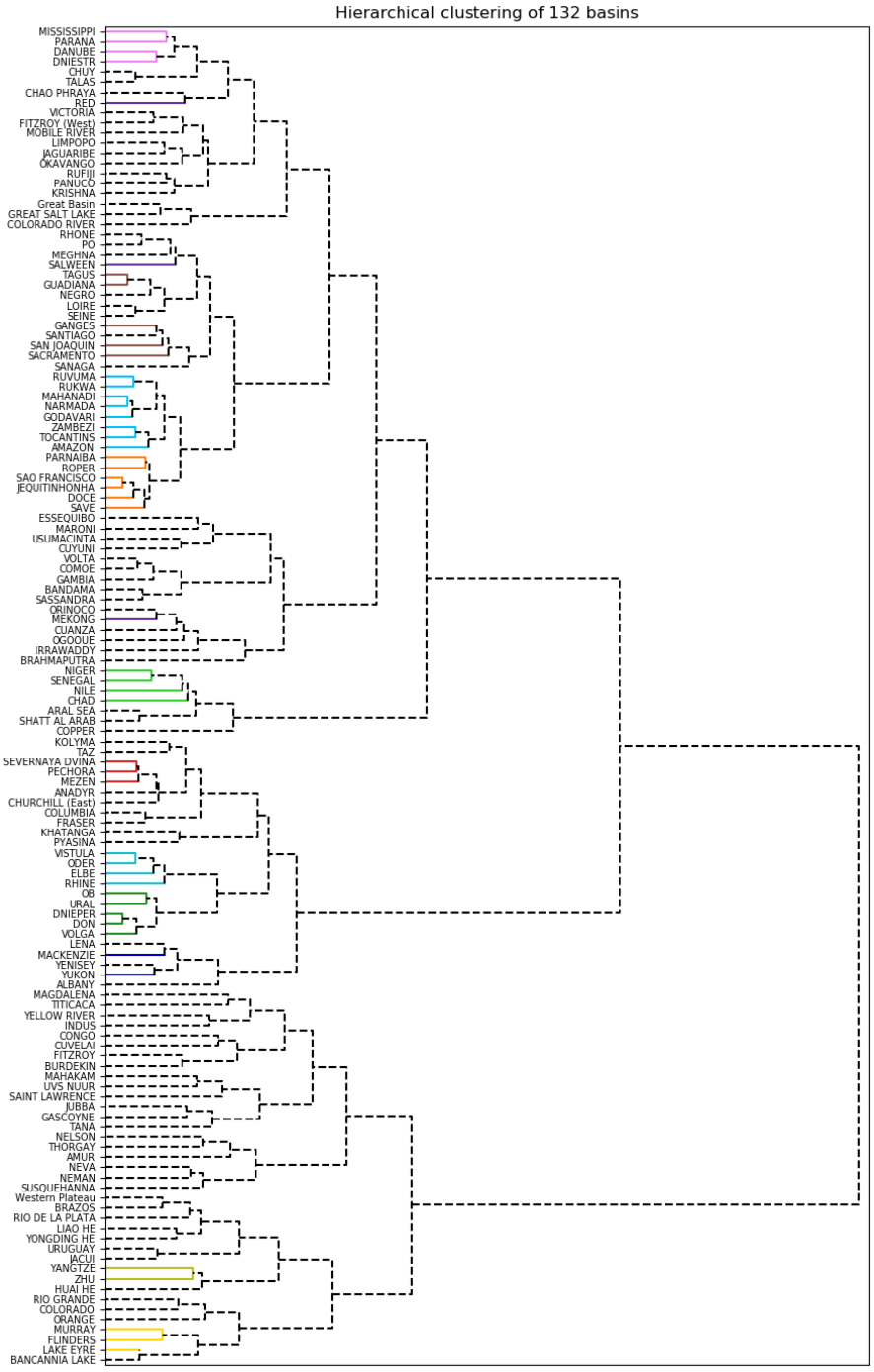

Figure S10. 132 basins with a maximum NSE larger than 0.8 or a maximum NSE_c larger than 0.1. The distance between basins is the Euclidean distance between the vector of costs for each combination. The height of the U-shaped link is proportional to this distance. Basins are clustered to minimize the intra-cluster variance and colored basins are those selected to plot Fig. **??**

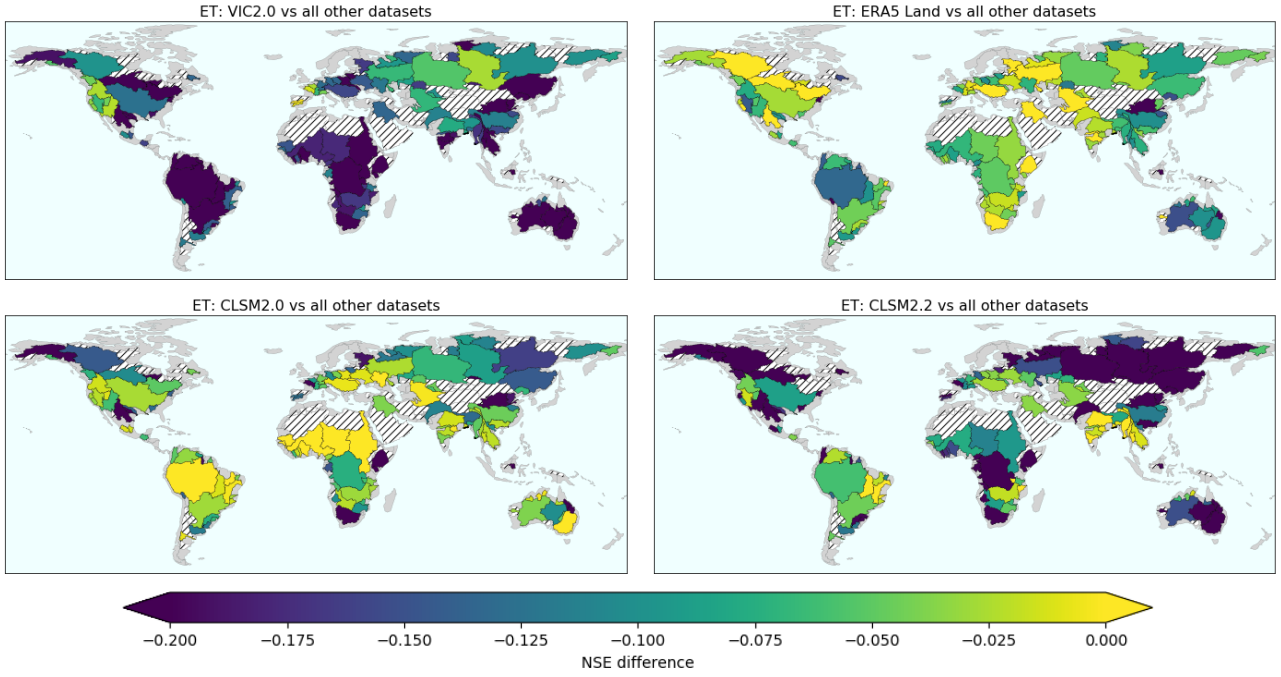

Figure S11. Same as **??** but for evapotranspiration datasets.

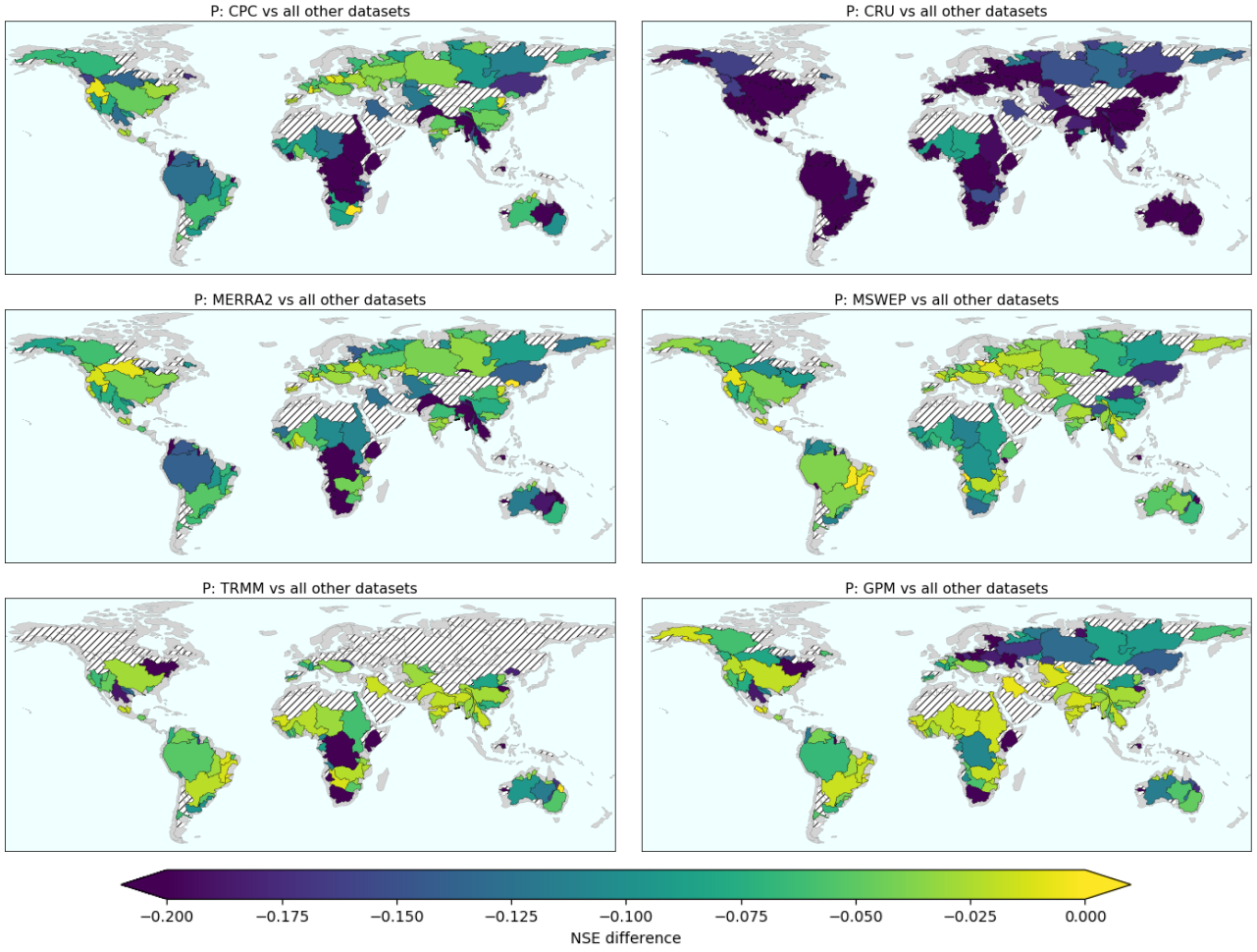

Figure S12. The mean of the 10th highest NSE with combinations comprising the reference dataset is compared to the mean of the 10th highest NSE excluding the reference dataset. Yellow indicates basins where the reference dataset is similar to or better than others while blues show regions where it was significantly worse. Hatches show basins with a poor water budget closure (maximum NSE lower than 0.8 and maximum NSE_c lower than 0.1).

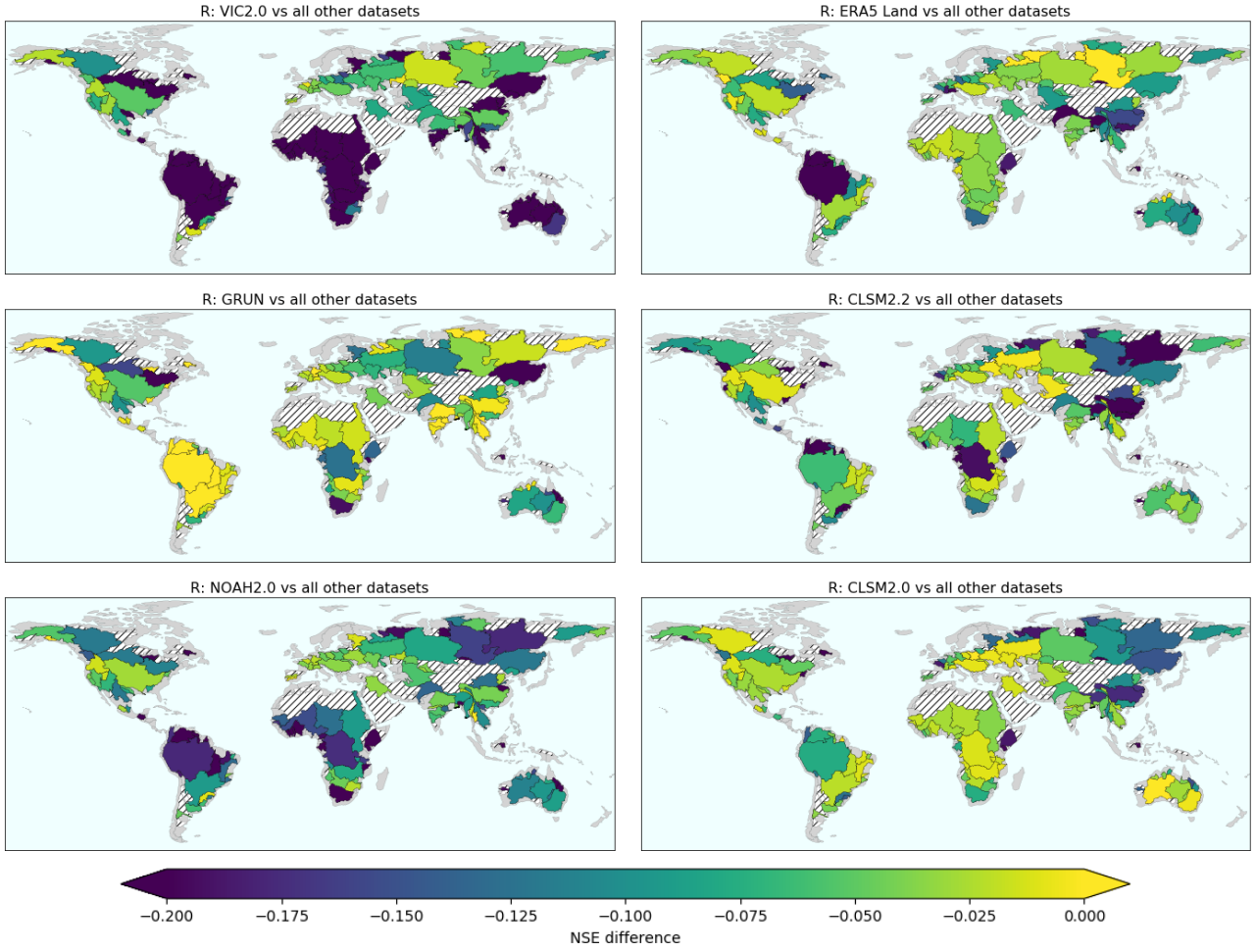

Figure S13. Same as **??** but for runoff datasets.

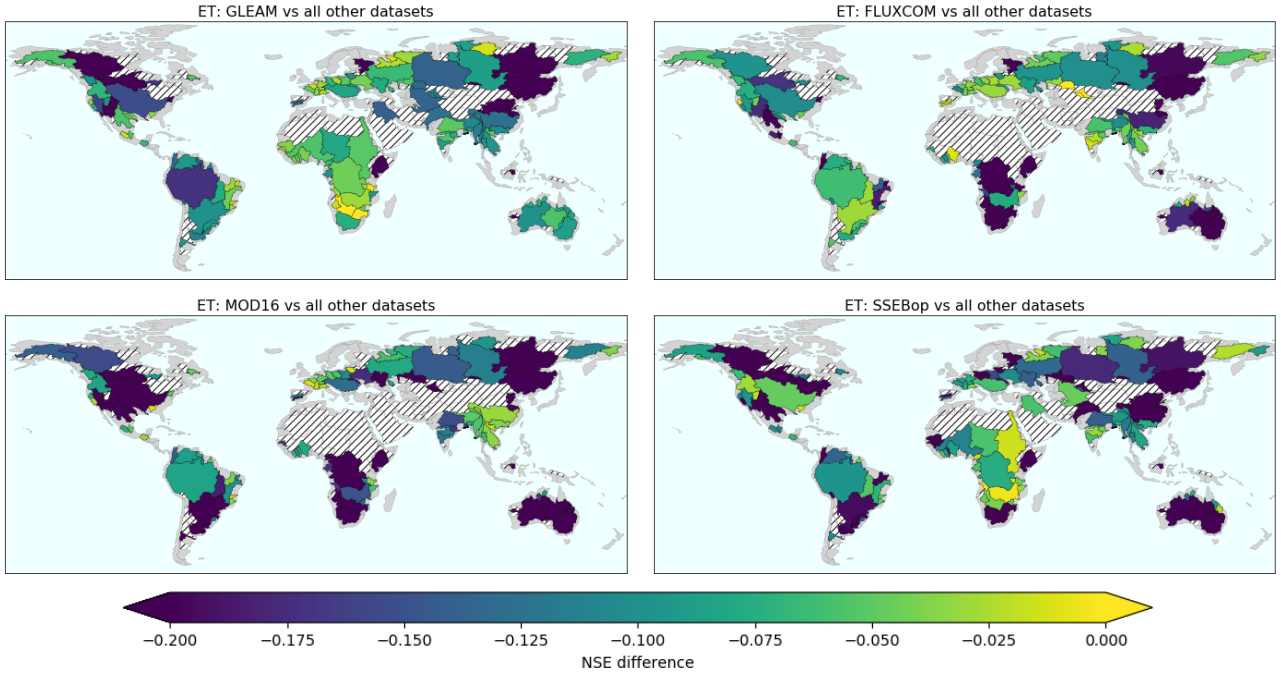

Figure S14. The mean of the 10th highest NSE with combinations comprising the reference dataset is compared to the mean of the 10th highest NSE excluding the reference dataset. Yellow indicates basins where the reference dataset is similar to or better than others while blues show regions where it was significantly worse. Hatches show basins with a poor water budget closure (maximum NSE lower than 0.8 and maximum NSE_c lower than 0.1).

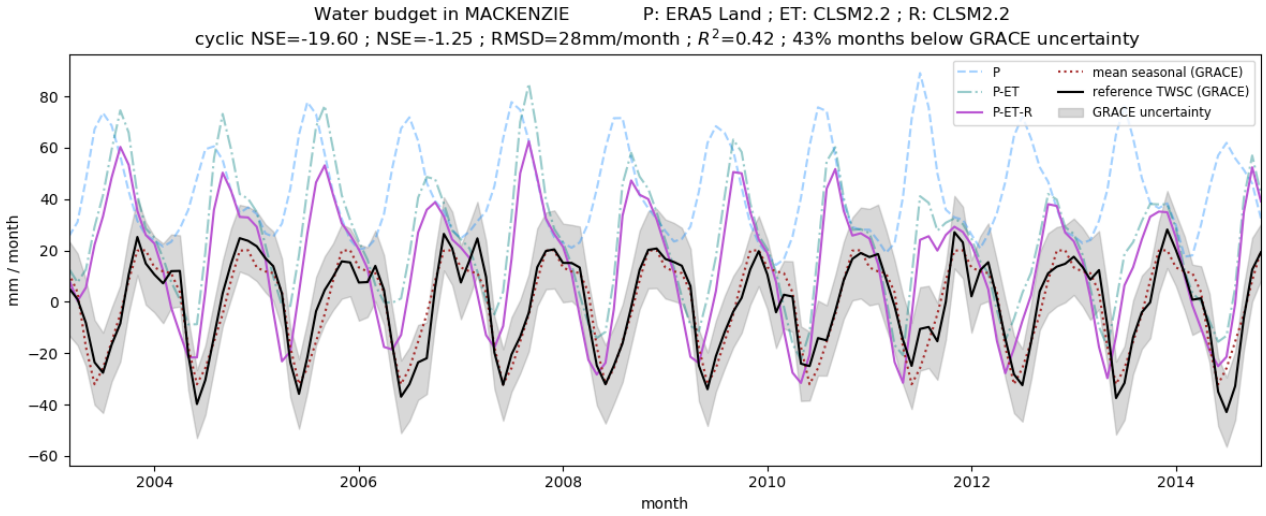

Figure S15. Components of the water budget in the Mackenzie basin with all components from GLDAS2.2 CLSM (assimilating GRACE TWS)

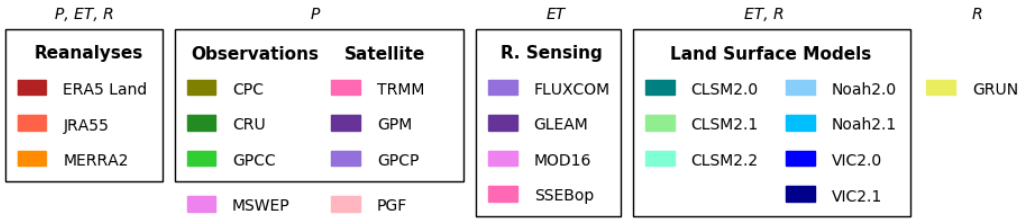

Figure S16. Legend of Fig. S17, S18, S19, S20

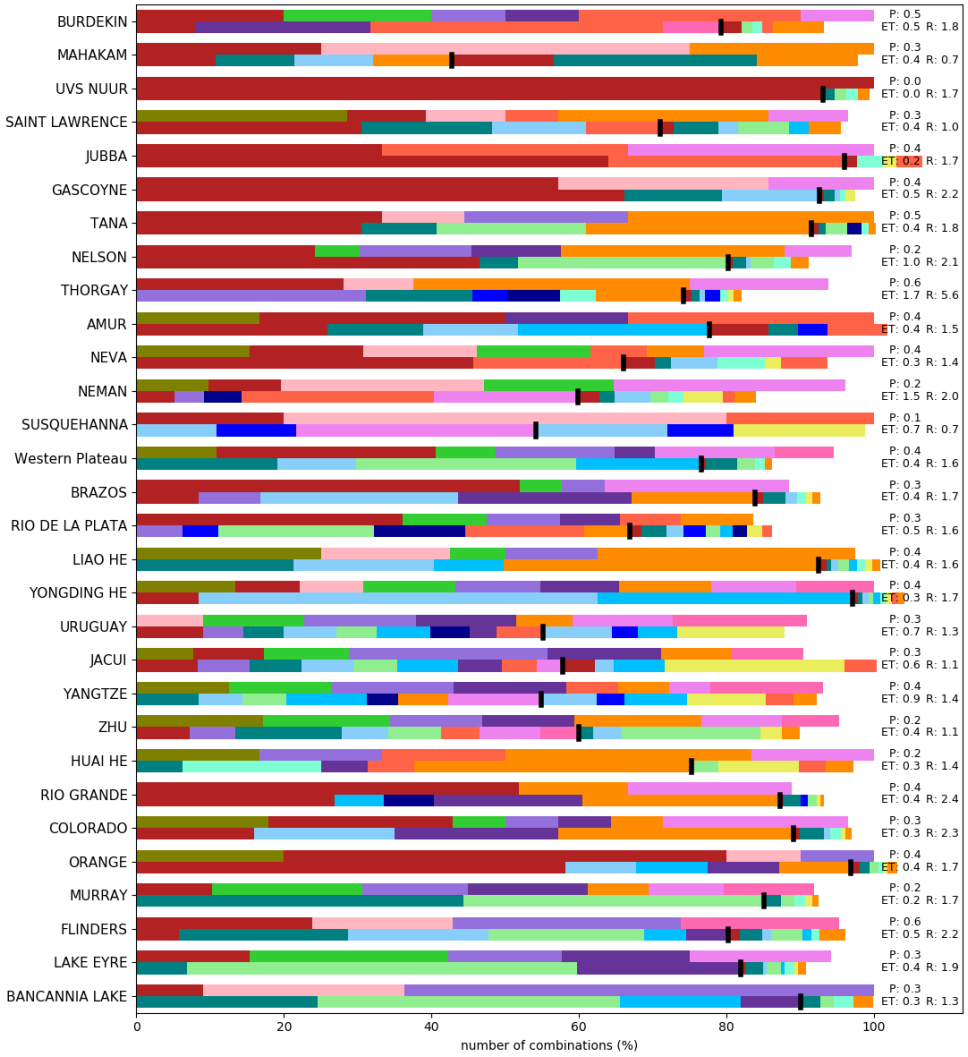

Figure S17. Datasets appearing in combinations that satisfy a cost lower than 0.1 for each basin separately. The top line of each basin bar represents precipitations datasets. The left part of the bottom line is evapotranspiration datasets while the right part is runoff. The limit between ET and R is symbolized by a black line located proportionally to the portion of ET in the mean annual water cycle of the corresponding region, explaining while the bottom line may have a length different than 100%. Basins are ordered according to hierarchical clustering (dendrogram in Fig. S10). The color legend for datasets can be found in Fig. S16

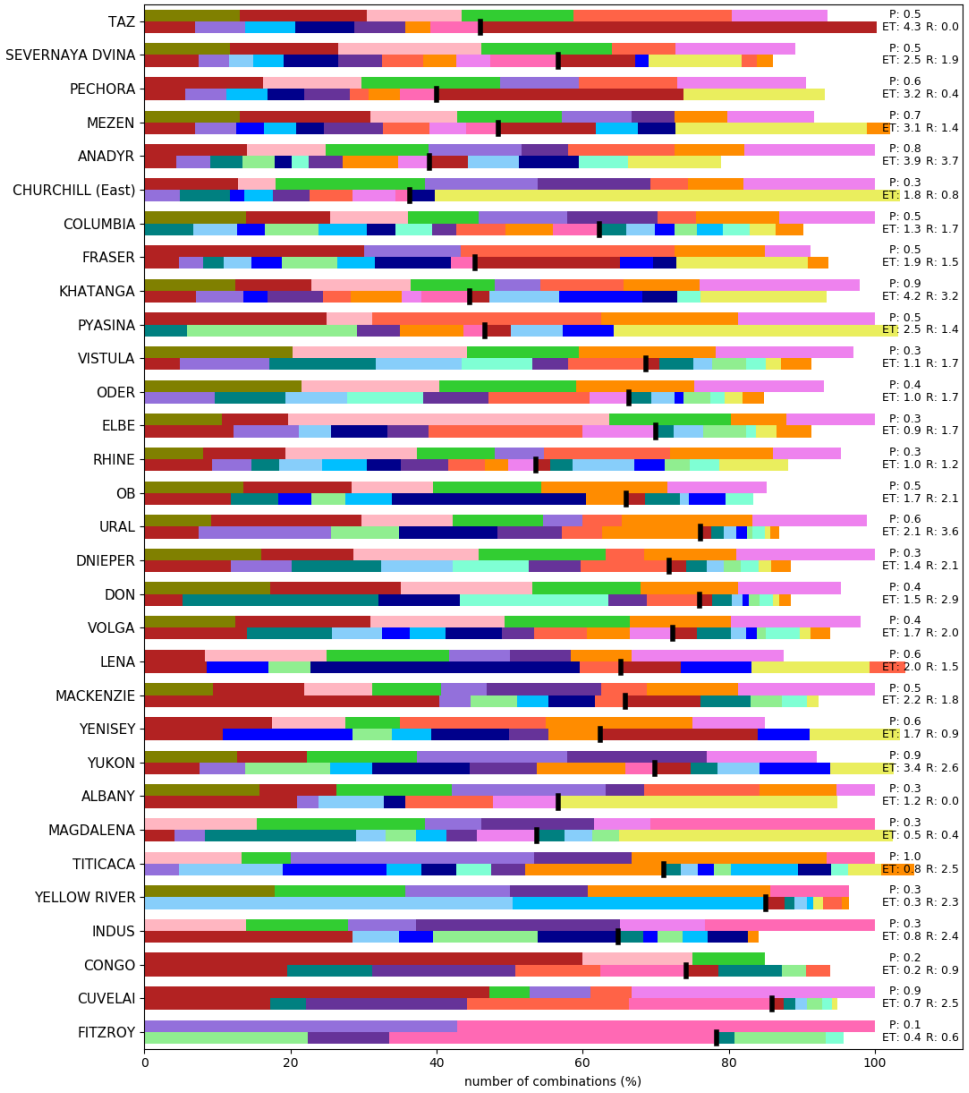

Figure S18. Following of Fig. S17

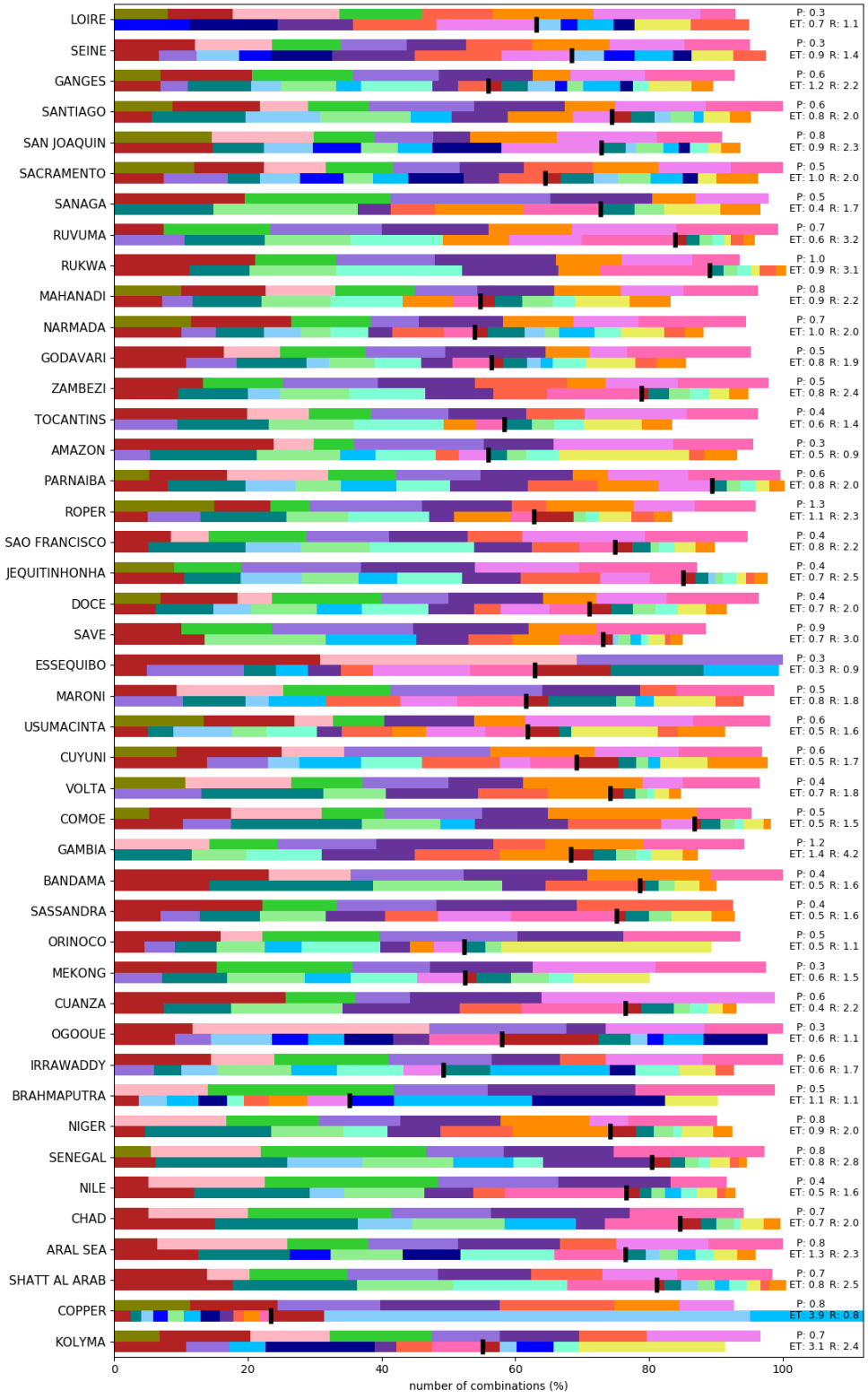

Figure S19. Following of Fig. S18

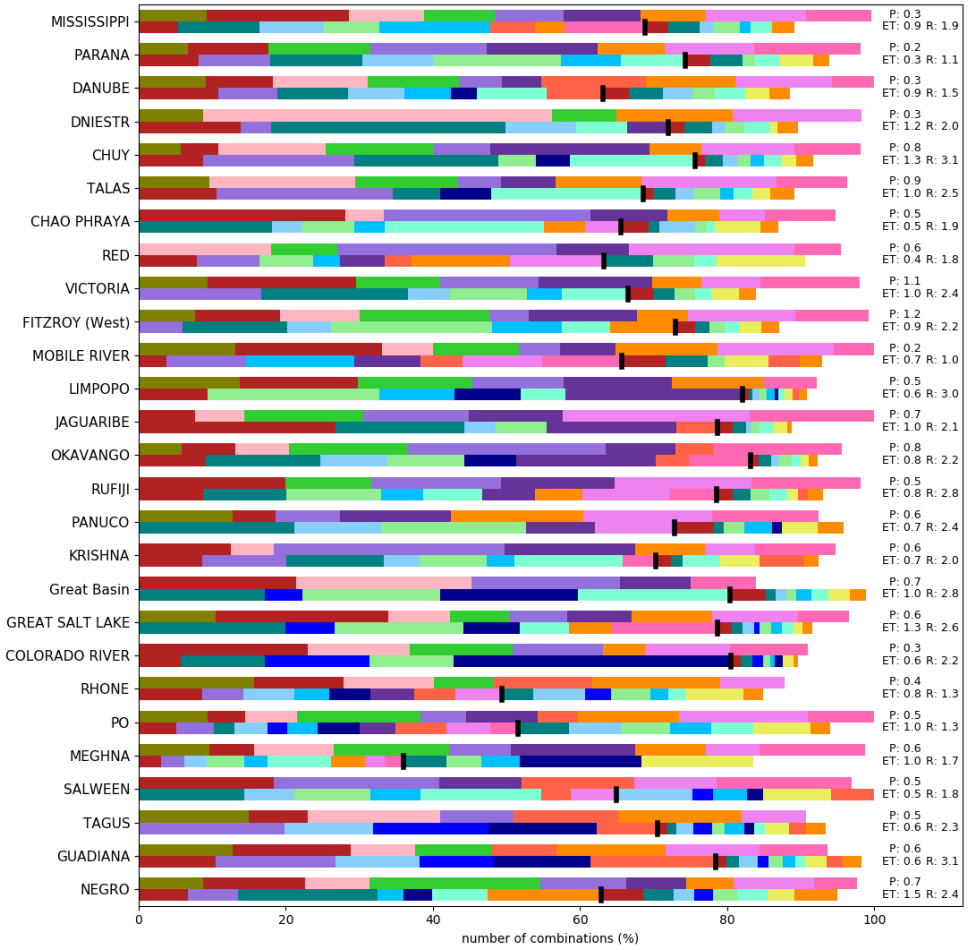

Figure S20. Following of Fig. S19

Additional tables

Table S1. Precipitations datasets

Name	Method	Period	Spatial resolution	Reference
CPC Unified	Rain-gauge	1979 - present	0.5°x 0.5°	Chen and Xie (2008)
CRU v4.04	Rain-gauge	1901 - 2019	0.5°x 0.5°	Harris et al. (2020)
GPCC v.2020	Rain-gauge	1891 - 2019	0.5°x 0.5°	Schneider et al. (2020)
GPCP v2.3	Rain-gauge and satellite	1979 - present	2.5°x 2.5°	Adler et al. (2018)
GPM IMERG v06	Satellite	2000 - present	0.1°x 0.1°	Huffman et al. (2019)
TRMM (TMPA/3B43)	Satellite	1998 - 2019	0.25°x 0.25°	Huffman et al. (2007, 2010)
ERA5 Land	Reanalysis	1981 - present	0.1°x 0.1°	Muñoz-Sabater (2019)
JRA55	Reanalysis	1958 - present	∼0.5°x 0.5°	Kobayashi et al. (2015); Harada et al. (2016)
MERRA2	Reanalysis	1980 - present	0.5°x 0.625°	Reichle et al. (2017)
PGF	Rain-gauge, Satellite, and Reanalyses	1948 - 2014	1.0°x 1.0°	Sheffield et al. (2006)
MSWEP v2.8	Rain-gauge, Satellite, and Reanalyses	1979 - present	0.1°x 0.1°	Beck et al. (2019)

Table S2. Evapotranspiration datasets

Name	Method	Period	Spatial resolution	Reference
GLDAS2.0 CLSM2.5	Land surface model	1948 - 2014	1.0°x 1.0°	Li et al. (2020a); Koster et al. (2000)
GLDAS2.1 CLSM2.5	Land surface model	2000 - 2020	1.0°x 1.0°	Li et al. (2020a); Koster et al. (2000)
GLDAS2.2 CLSM2.5	Land surface model	2003 - 2020	0.25°x 0.25°	Li et al. (2019, 2020a)
GLDAS2.0 NOAH3.6	Land surface model	1948 - 2014	1.0°x 1.0°	Beaudoing et al. (2019); Chen et al. (1996)
GLDAS2.1 NOAH3.6	Land surface model	2000 - 2020	1.0°x 1.0°	Beaudoing et al. (2019); Chen et al. (1996)
GLDAS2.0 VIC4.1.2	Land surface model	1948 - 2014	1.0°x 1.0°	Beaudoing et al. (2020); Liang et al. (1994)
GLDAS2.1 VIC4.1.2	Land surface model	2000 - 2020	1.0°x 1.0°	Beaudoing et al. (2020); Liang et al. (1994)
FLUXCOM	Machine learning (remote sensing only)	2001 - 2015	0.5°x 0.5°	Jung et al. (2019)
GLEAM v3.3a	Priestley-Taylor	1980 - 2018	0.25°x 0.25°	Martens et al. (2017); Miralles et al. (2011)
MOD16	Penman-Monteith	2000-2015	0.5°x 0.5°	Mu et al. (2011)
SSEBop	Surface energy balance	2003 - 2020	0.5°x 0.5°	Senay et al. (2013)
ERA5 Land	Reanalysis (Penman-Monteith)	1981 - present	0.1°x 0.1°	Muñoz-Sabater (2019)
JRA55	Reanalysis (JMA Simple Biosphere SiB)	1958 - present	0.5°x 0.5°	Kobayashi et al. (2015); Harada et al. (2016)
MERRA2	Reanalysis (Penman-Monteith)	1980 - present	0.5°x 0.625°	Gelaro et al. (2017)

Table S3. Components of the mean annual water cycle in Pacific islands

	P (mm/year)	ET (mm/year)	R (mm/year)
SEPIK	3390 ± 653	1404 ± 223	2116 ± 597
MAMBERAMO	3578 ± 851	1340 ± 227	2406 ± 756
MAHAKAM	3163 ± 356	1359 ± 272	1911 ± 529
KAPUAS	3666 ± 204	1366 ± 266	2339 ± 480

The first value is the mean annual cycle averaged over all datasets while the second one is the standard deviation of mean annual values over all datasets

Table S4. Components of the mean annual water cycle in equatorial rain forest/monsoon basins in South America

	P (mm/year)	ET (mm/year)	R (mm/year)
MAGDALENA	2339 ± 650	1157 ± 216	1373 ± 498
CUYUNI	2051 ± 269	1395 ± 223	766 ± 327
ESSEQUIBO	2121 ± 251	1314 ± 217	946 ± 405
MARONI	2312 ± 247	1406 ± 269	885 ± 364
AMAZON	2177 ± 172	1251 ± 196	958 ± 251
ORINOCO	2269 ± 289	1237 ± 200	1090 ± 315

The first value is the mean annual cycle averaged over all datasets while the second one is the standard deviation of mean annual values over all datasets

Table S5. Values of NSE and cyclostationary NSE using GRDC as the only runoff dataset compared to the maximum over all other runoff datasets.

Basin name	maximum NSE with all sources of runoff	maximum NSE with GRDC runoff	maximum NSE_c with all sources of runoff	maximum NSE_c with GRDC runoff	months among 2003-2014 with available runoff data (in %)
AMAZON	0.90	0.98	-1.49	0.49	100.0
AMUR	0.59	0.90	0.46	0.87	31.9
CONGO	0.86	0.87	0.18	0.22	66.0
DANUBE	0.90	NaN	0.63	NaN	0.0
LENA	0.83	NaN	-0.23	NaN	0.0
MACKENZIE	0.89	0.91	-0.01	0.19	100.0
MISSISSIPPI	0.93	0.94	0.47	0.53	84.4
OB	0.92	0.96	0.23	0.61	66.0
ORANGE	0.34	0.20	0.20	0.03	100.0
PARANA	0.90	0.90	0.69	0.68	95.0
VOLGA	0.92	0.94	0.45	0.58	66.0
YANGTZE	0.75	NaN	0.21	NaN	7.1
YELLOW RIVER	0.74	NaN	0.50	NaN	7.1
YENISEY	0.92	0.94	0.27	0.41	74.5
YUKON	0.90	0.93	0.11	0.36	100.0

From the large basins used in Li et al. (2020b), only those with an area matching the discharge area from GRDC gauge stations were selected. The maximum NSE (resp. NSE_c) with GRDC runoff was computed over combinations of P and ET from all available datasets, and R from GRDC measurements in basins with at least 66% of months available. In basins with less available months, Nan refers to no computation. The two other columns are the maximum over the 1694 combinations of all P, ET, and R datasets.

References

Adler, R. F., Sapiano, M. R. P., Huffman, G. J., Wang, J.-J., Gu, G., Bolvin, D., Chiu, L., Schneider, U., Becker, A., Nelkin, E., Xie, P., Ferraro, R., and Shin, D.-B.: The Global Precipitation Climatology Project (GPCP) Monthly Analysis (New Version 2.3) and a Review of 2017 Global Precipitation, Atmosphere, 9, https://doi.org/10.3390/atmos9040138, 2018.

Beaudoing, H., Rodell, M., and NASA/GSFC/HSL: GLDAS Noah Land Surface Model L4 monthly 1.0 x 1.0 degree, Version 2.0, https://doi.org/10.5067/QN80TO7ZHFJZ, type: dataset, 2019.

Beaudoing, H., Rodell, M., and NASA/GSFC/HSL: GLDAS VIC Land Surface Model L4 monthly 1.0 x 1.0 degree V2.0, https://doi.org/10.5067/ZRIHVF29X43C, type: dataset, 2020.

Beck, H. E., Wood, E. F., Pan, M., Fisher, C. K., Miralles, D. G., van Dijk, A. I. J. M., McVicar, T. R., and Adler, R. F.: MSWEP V2 Global 3-Hourly 0.1° Precipitation: Methodology and Quantitative Assessment, Bulletin of the American Meteorological Society, 100, 473–500, https://doi.org/10.1175/BAMS-D-17-0138.1, 2019.

Chen, F., Mitchell, K., Schaake, J., Xue, Y., Pan, H.-L., Koren, V., Duan, Q. Y., Ek, M., and Betts, A.: Modeling of land surface evaporation by four schemes and comparison with FIFE observations, Journal of Geophysical Research: Atmospheres, 101, 7251–7268, https://doi.org/10.1029/95JD02165, 1996.

Chen, M. and Xie, P.: CPC Unified Gauge-based Analysis of Global Daily Precipitation, Cairns, Australia, 2008.

Gelaro, R., McCarty, W., Suárez, M. J., Todling, R., Molod, A., Takacs, L., Randles, C. A., Darmenov, A., Bosilovich, M. G., Reichle, R., Wargan, K., Coy, L., Cullather, R., Draper, C., Akella, S., Buchard, V., Conaty, A., da Silva, A. M., Gu, W., Kim, G.-K., Koster, R., Lucchesi, R., Merkova, D., Nielsen, J. E., Partyka, G., Pawson, S., Putman, W., Rienecker, M., Schubert, S. D., Sienkiewicz, M., and Zhao, B.: The Modern-Era Retrospective Analysis for Research and Applications, Version 2 (MERRA-2), Journal of Climate, 30, 5419–5454, https://doi.org/10.1175/JCLI-D-16-0758.1, 2017.

Harada, Y., Kamahori, H., Kobayashi, C., Endo, H., Kobayashi, S., Ota, Y., Onoda, H., Onogi, K., Miyaoka, K., and Takahashi, K.: The JRA-55 Reanalysis: Representation of Atmospheric Circulation and Climate Variability, Journal of the Meteorological Society of Japan. Ser. II, 94, 269–302, https://doi.org/10.2151/jmsj.2016-015, 2016.

Harris, I., Osborn, T. J., Jones, P., and Lister, D.: Version 4 of the CRU TS monthly high-resolution gridded multivariate climate dataset, Scientific Data, 7, 109, https://doi.org/10.1038/s41597-020-0453-3, 2020.

Huffman, G. J., Bolvin, D. T., Nelkin, E. J., Wolff, D. B., Adler, R. F., Gu, G., Hong, Y., Bowman, K. P., and Stocker, E. F.: The TRMM Multisatellite Precipitation Analysis (TMPA): Quasi-Global, Multiyear, Combined-Sensor Precipitation Estimates at Fine Scales, Journal of Hydrometeorology, 8, 38–55, https://doi.org/10.1175/JHM560.1, 2007.

Huffman, G. J., Adler, R. F., Bolvin, D. T., and Nelkin, E. J.: The TRMM Multi-Satellite Precipitation Analysis (TMPA), in: Gebremichael M., Hossain F. (eds) Satellite rainfall Applications for Surface Hydrology, pp. 3–22, Springer, Dordrecht, https://doi.org/10.1007/978-90-481-2915-7_1, 2010.

Huffman, G. J., Bolvin, D. T., Braithwaite, D., Hsu, K., Joyce, R., Kidd, C., Nelkin, E. J., Sorooshian, S., Tan, J., and Xie, P.: NASA Global Precipitation Measurement (GPM) Integrated Multi-Satellite Retrievals for GPM (IMERG), p. 38, https://doi.org/10.5067/GPM/IMERG/3B-MONTH/06, 2019.

Jung, M., Koirala, S., Weber, U., Ichii, K., Gans, F., Camps-Valls, G., Papale, D., Schwalm, C., Tramontana, G., and Reichstein, M.: The FLUXCOM ensemble of global land-atmosphere energy fluxes, Scientific Data, 6, 74, https://doi.org/10.1038/s41597-019-0076-8, 2019.

Kobayashi, S., Ota, Y., Harada, Y., Ebita, A., Moriya, M., Onoda, H., Onogi, K., Kamahori, H., Kobayashi, C., Endo, H., Miyaoka, K., and Takahashi, K.: The JRA-55 Reanalysis: General Specifications and Basic Characteristics, Journal of the Meteorological Society of Japan. Ser. II, 93, 5–48, https://doi.org/10.2151/jmsj.2015-001, 2015.

Koster, R. D., Suarez, M. J., Ducharne, A., Stieglitz, M., and Kumar, P.: A catchment-based approach to modeling land surface processes in a general circulation model: 1. Model structure, Journal of Geophysical Research: Atmospheres, 105, 24 809–24 822, https://doi.org/10.1029/2000JD900327, 2000.

Li, B., Rodell, M., Kumar, S., Beaudoing, H. K., Getirana, A., Zaitchik, B. F., Goncalves, L. G., Cossetin, C., Bhanja, S., Mukherjee, A., Tian, S., Tangdamrongsub, N., Long, D., Nanteza, J., Lee, J., Policelli, F., Goni, I. B., Daira, D., Bila, M., Lannoy, G., Mocko, D., Steele-Dunne, S. C., Save, H., and Bettadpur, S.: Global GRACE Data Assimilation for Groundwater and Drought Monitoring: Advances and Challenges, Water Resources Research, 55, 7564–7586, https://doi.org/10.1029/2018WR024618, 2019.

Li, B., Beaudoing, H., Rodell, M., and NASA/GSFC/HSL: GLDAS Catchment Land Surface Model L4 monthly 1.0 x 1.0 degree V2.0, https://doi.org/10.5067/SGSL3LNKGJWW, type: dataset, 2020a.

Li, F., Kusche, J., Rietbroek, R., Wang, Z., Forootan, E., Schulze, K., and Lück, C.: Comparison of Data-Driven Techniques to Reconstruct (1992–2002) and Predict (2017–2018) GRACE-Like Gridded Total Water Storage Changes Using Climate Inputs, Water Resources Research, 56, https://doi.org/10.1029/2019WR026551, 2020b.

Liang, X., Lettenmaier, D. P., Wood, E. F., and Burges, S. J.: A simple hydrologically based model of land surface water and energy fluxes for general circulation models, Journal of Geophysical Research, 99, 14 415, https://doi.org/10.1029/94JD00483, 1994.

Martens, B., Miralles, D. G., Lievens, H., van der Schalie, R., de Jeu, R. A. M., Fernández-Prieto, D., Beck, H. E., Dorigo, W. A., and Verhoest, N. E. C.: GLEAM v3: satellite-based land evaporation and root-zone soil moisture, Geoscientific Model Development, 10, 1903–1925, https://doi.org/10.5194/gmd-10-1903-2017, 2017.

Miralles, D. G., Holmes, T. R. H., De Jeu, R. A. M., Gash, J. H., Meesters, A. G. C. A., and Dolman, A. J.: Global land-surface evaporation estimated from satellite-based observations, Hydrology and Earth System Sciences, 15, 453–469, https://doi.org/10.5194/hess-15-453-2011, 2011.

Mu, Q., Zhao, M., and Running, S. W.: Improvements to a MODIS global terrestrial evapotranspiration algorithm, Remote Sensing of Environment, 115, 1781–1800, https://doi.org/10.1016/j.rse.2011.02.019, 2011.

Muñoz-Sabater, J.: ERA5-Land monthly averaged data from 2001 to present, ECMWF, https://doi.org/10.24381/CDS.68D2BB30, type: dataset, 2019.

Reichle, R. H., Liu, Q., Koster, R. D., Draper, C. S., Mahanama, S. P. P., and Partyka, G. S.: Land Surface Precipitation in MERRA-2, Journal of Climate, 30, 1643–1664, https://doi.org/10.1175/JCLI-D-16-0570.1, 2017.

Schneider, U., Becker, A., Finger, P., Rustemeier, E., and Ziese, M.: GPCC Full Data Monthly Version 2020 at 0.5°, https://doi.org/10.5676/DWD_GPCC/FD_M_V2020_050, 2020.

Senay, G. B., Bohms, S., Singh, R. K., Gowda, P. H., Velpuri, N. M., Alemu, H., and Verdin, J. P.: Operational Evapotranspiration Mapping Using Remote Sensing and Weather Datasets: A New Parameterization for the SSEB Approach, JAWRA Journal of the American Water Resources Association, 49, 577–591, https://doi.org/10.1111/jawr.12057, 2013.

Sheffield, J., Goteti, G., and Wood, E. F.: Development of a 50-Year High-Resolution Global Dataset of Meteorological Forcings for Land Surface Modeling, Journal of Climate, 19, 3088–3111, https://doi.org/10.1175/JCLI3790.1, place: Boston MA, USA Publisher: American Meteorological Society, 2006.